Anisotropy-Driven Instability in Intense Charged Particle Beams*

Edward A. Startsev, Ronald C. Davidson and Hong Qin
Plasma Physics Laboratory, Princeton University, Princeton, New Jersey 08543

Abstract

We have generalized the analysis of the classical Harris instability to the case of a one-component intense charged particle beam with anisotropic temperature including the important effects of finite transverse geometry and beam space-charge. For a long, coasting beam, the delta-f particle-in-cell code BEST and the eighenmode code bEASt have been used to determine detailed 3D stability properties over a wide range of temperature anisotropy and beam intensity. A theoretical model is developed based on the Vlasov-Maxwell equations which describes the essential features of the linear stage of this instability. Both the simulations and the analytical theory clearly show that moderately intense beams are linearly unstable to short-wavelength perturbations provided the ratio of the longitudinal temperature to the transverse temperature is smaller than some threshold value.

INTRODUCTION

It is well known that in electrically neutral plasmas with uniform magnetic field and strongly anisotropic electron distribution ($T_{||e}/T_{\perp e} \ll 1$), where subscript $||(\perp)$ denotes parallel (perpendicular) to the magnetic field, an electrostatic (Harris-like) collective instability may develop if the plasma is sufficiently dense that $\omega_{pe} > \omega_{ce}$, where $\omega_{pe} = (4\pi e^2 n/m)^{1/2}$ is the electron plasma frequency, and $\omega_{ce} = eB/mc$ is the electron cyclotron frequency [1]. Such conditions develop naturally in accelerators. Indeed, due to the conservation of energy for particles with charge e_b and mass m_b accelerated by a voltage V, the energy spread of particles in the beam does not change, and (nonrelativistically) $\Delta E_{bi} = m_b \Delta v_{bi}^2/2 = \Delta E_{bf} = m_b V_b \Delta v_{bf}$, where $V_b = (2e_b V/m_b)^{1/2}$ is the average beam velocity after acceleration. Therefore, the velocity spread-squared, or equivalently the temperature, changes according to $T_{||bf} = T_{||bi}^2/2e_b V$ (for a nonrelativistic beam). In addition, the transverse temperature may increase due to nonlinearities in the applied focusing field, the self-field forces, nonstationary beam profiles, and beam mismatch. For the case of charged particle beams in accelerators, the cyclotron oscillations in the applied magnetic field are replaced by the betatron oscillations of the beam particles in the combined applied and self-generated fields [2, 3, 4, 5, 6, 7, 8, 9, 10, 11, 12]. Heavy ion fusion experiments require transporting high-current beams when the average depressed betatron frequency of the beam particles is much smaller than the average plasma frequency of the beam particles. The resulting anisotropy-driven instability may lead to a detoriation of the beam quality and an increase in the longitudinal velocity spread, which would make focusing the beam difficult and impose a limit on the minimum spot size achievable in heavy ion fusion experiments.

* Research supported by the U. S. Department of Energy.

SIMPLIFIED MODEL OF ELECTROSTATIC HARRIS-TYPE INSTABILITY

For simplicity, the analysis is carried out in the beam frame ($V_b = 0$). In what follows, it is convenient to introduce the effective *depressed* betatron frequency $\omega_{\beta\perp}$ defined by

$$\omega_{\beta\perp}^2 = \frac{2T_{\perp b}}{m_b r_b^2} = \omega_f^2 - \bar{\omega}_{pb}^2/2, \tag{1}$$

where $T_{\perp b}$ is the transverse beam temperature, r_b is the root-mean-square beam radius, m_b is the mass of a beam particle, and

$$\bar{\omega}_{pb}^2 = \frac{4\pi e_b^2}{m_b r_b^2} \int_0^{r_w} dr r n_b(r) \tag{2}$$

is the average beam plasma frequency-squared. The normalized tune depression $\bar{\nu}/\nu_0$ is defined by

$$\frac{\bar{\nu}}{\nu_0} \equiv \frac{\omega_{\beta\perp}}{\omega_f}, \tag{3}$$

where $\omega_f = const.$ is the transverse frequency associated with the applied focusing field in the smooth-focusing approximation.

We now briefly illustrate the physical mechanism for the electrostatic Harris instability in intense particle beams with a Kapchinskij – Vladimirskij (KV) distribution. As shown in previous studies [9, 10, 11, 12], the dipole mode has the highest growth rate, and for $T_{||b} = 0$ the growth rate is an increasing function of $k_z r_b$ and approaches a maximum value for $k_z^2 r_b^2 \gg 1$. Therefore, we consider dipole-mode perturbations with $k_z^2 r_b^2 \gg 1$, which in lowest order correspond to a rigid displacement of the beam centroid in the transverse x-direction (for example) with perturbed electric field given approximately by $\delta\mathbf{E} = -ik_z \delta\phi \hat{\mathbf{e}}_z$. Since a KV beam has a uniform density profile, the perturbed electrostatic potential inside the beam has the form

$$\delta\phi(\mathbf{x}, t) = \hat{\phi} \frac{x}{r_b} \exp(ik_z z - i\omega t), \tag{4}$$

where $\hat{\phi}$ is the perturbation amplitude, and ω and k_z are the perturbation frequency and the longitudinal wavenumber, respectively.

Next, we consider a beam particle oscillating longitudinally in the perturbed electric field and at the same time performing transverse betatron oscillations. For general distribution function, the equilibrium self-electric field is nonlinear, and the transverse betatron oscillation of the beam particles will contain many harmonics of the betatron frequency, which generally depends on the particle energy and angular momentum [9, 11, 12]. For purposes of illustrating the physical mechanism, we consider here the simplified model of an equivalent KV beam where all of the particles oscillate with the same frequency, equal to the average depressed betatron frequency $\omega_{\beta\perp}$ defined in Eq. (1), i.e.,

$$x(t) = \hat{x}\cos(\omega_{\beta\perp}t + \alpha_0), \tag{5}$$

where α_0 is the oscillation phase at $t = 0$, $\hat{x} = \sqrt{2H_x/m_b}/\omega_{\beta\perp}$ is the oscillation amplitude, and H_x is the transverse energy.

Making use of Eqs. (4) and (5), the longitudinal equation of motion for a beam particle becomes

$$\ddot{z} = -ik_z\frac{e_b}{m_b}\hat{\phi}\frac{\hat{x}}{r_b}\cos(\omega_{\beta\perp}t+\alpha_0)\exp(ik_z z_0 - i\omega t), \tag{6}$$

where we have assumed that beam is cold in the longitudinal direction. Integrating Eq. (6) with respect to time t, we obtain

$$\begin{aligned} z_\alpha &= ik_z\frac{e_b}{m_b}\hat{\phi}\frac{\hat{x}}{2r_b}\left[\frac{\exp(i\alpha)}{(\omega-\omega_{\beta\perp})^2}\right. \\ &+ \left.\frac{\exp(-i\alpha)}{(\omega+\omega_{\beta\perp})^2}\right]\exp(ik_z z_0 - i\omega t), \end{aligned} \tag{7}$$

where $\alpha = \alpha_0 + \omega_{\beta\perp}t$. To calculate the average displacement $\langle z\rangle(x,z,t)$ in the z direction we average over all particles with the same transverse position x at time t. This gives

$$\begin{aligned} \langle z\rangle(x,z,t) &= \frac{1}{2}(z_\alpha + z_{-\alpha}) \\ &= -\frac{e_b\delta E_z}{2m_b}\left[\frac{1}{(\omega-\omega_{\beta\perp})^2} + \frac{1}{(\omega+\omega_{\beta\perp})^2}\right], \end{aligned} \tag{8}$$

where $\delta E_z = -ik_z\delta\phi$ [see Eq. (4)]. Note that even though the individual particle motion [Eq. (7)] has two characteristic frequencies, $\omega-\omega_{\beta\perp}$ and $\omega+\omega_{\beta\perp}$, the average quantity $\langle z\rangle$ oscillates at the perturbation frequency ω [Eq. (8)]. From the continuity equation for the density perturbation,

$$\frac{\partial\delta n_b}{\partial t} + \frac{\partial}{\partial z}\left(n_b^0\frac{\partial\langle z\rangle}{\partial t}\right) = 0, \tag{9}$$

we obtain

$$\delta n_b = -n_0\frac{\partial\langle z\rangle}{\partial z}. \tag{10}$$

Substituting Eqs. (8) and (10) into Poisson's equation $\nabla\cdot\delta\mathbf{E} \simeq \partial\delta E_z/\partial z = 4\pi e_b\delta n_b$, we obtain the simple dispersion relation

$$1 = \frac{\bar{\omega}_{pb}^2}{2}\left[\frac{1}{(\omega-\omega_{\beta\perp})^2} + \frac{1}{(\omega+\omega_{\beta\perp})^2}\right], \tag{11}$$

where has been made use of the average value of the plasma frequency introduced in Eq. (2) to take into account the beam density profile shape in a lowest-order sense. Using the definition of the depressed tune [Eqs. (1) and (3)], we can rewrite Eq. (11) as

$$\frac{\nu_n^2}{1-\nu_n^2} = \left[\frac{1}{(\omega_n/\nu_n-1)^2} + \frac{1}{(\omega_n/\nu_n+1)^2}\right], \tag{12}$$

where $\nu_n = \bar{\nu}/\nu_0$ is the normalized depressed tune, and $\omega_n = \omega/\omega_f$ is the normalized mode frequency. Equation (12) is easily solved to give

$$\omega_n^2 = 1 \pm \sqrt{(1-\nu_n^2)(1+3\nu_n^2)}. \tag{13}$$

From Eq. (13), we determine that the mode with the lower sign in Eq. (13) is unstable and purely growing for $\nu_n < \nu_n^{th} = \sqrt{2/3} \approx 0.82$, with maximum growth rate $(Im\omega)^{max}/\omega_f = \sqrt{2/\sqrt{3}-1} \approx 0.39$ occurring for $\nu_n^{max} = \sqrt{1/3} \approx 0.58$. Also, for very intense beams with $\nu_n \to 0$, the normalized growth rate becomes $(Im\omega)/\omega_f \simeq \bar{\nu}/\nu_0$. In Fig. 1(a), the normalized growth rate $(Im\omega)/\omega_f$, plotted as a function of the normalized tune depression $\bar{\nu}/\nu_0$ [Eq. (13)], is compared with detailed numerical simulation results [11, 12]. Despite the approximations made in the present simplified model, the agreement is reasonably good.

SIMULATION STUDIES OF THE TEMPERATURE-ANISOTROPY INSTABILITY

For an arbitrary equilibrium distribution one cannot solve the stability problem analytically and must employ numerical techniques. In our previous studies of the temperature-anisotropy instability we used the linear eighenmode method as implemented in the Beam Eigenmode and Spectra (bEASt) Code [12], and the particle-in-cell δf method as implemented in Beam Equilibrium, Stability and Transport (BEST) code [9, 10, 11, 13] to investigate the detailed linear properties of the instability for perturbations about an anisotropic thermal equilibrium distribution ($T_{\perp b} > T_{\|b}$) described in the beam frame ($V_b = 0$ and $\gamma_b = 1$) by the self-consistent axisymmetric Vlasov equilibrium

$$f_b^0(r,\mathbf{p}) = \frac{\widehat{n}_b}{(2\pi m_b)^{3/2}T_{\perp b}T_{||b}^{1/2}}\exp\left(-\frac{H_\perp}{T_{\perp b}} - \frac{p_z^2}{2m_bT_{\|b}}\right). \tag{14}$$

Here, $H_\perp = p_\perp^2/2m_b + (1/2)m_b\omega_f^2(x^2+y^2) + e_b\phi^0(r)$ is the single-particle Hamiltonian for the transverse particle motion, $p_\perp = (p_x^2+p_y^2)^{1/2}$ is the transverse particle momentum, $r = (x^2+y^2)^{1/2}$ is the radial distance from the beam axis, and $\phi^0(r)$ is the equilibrium space-charge potential determined self-consistently from Poisson's equation,

$$\frac{1}{r}\frac{\partial}{\partial r}\left(r\frac{\partial\phi^0}{\partial r}\right) = -4\pi e_b n_b^0, \tag{15}$$

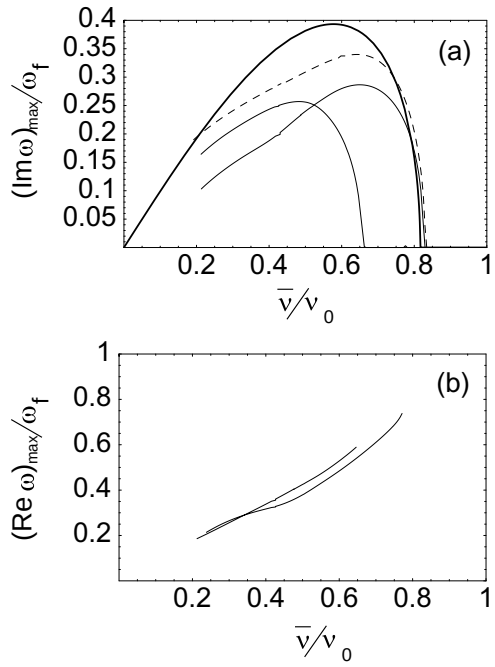

Figure 1: Plots of the normalized growth rate $(Im\omega)_{max}/\omega_f$ and real frequency $(Re\omega)_{max}/\omega_f$ at maximum growth versus normalized tune depression $\bar{\nu}/\nu_0$ for $T_{||b}/T_{\perp b} = 0$ and m=0 (solid curve) and m=1 (dotted curve). The thick solid curve corresponds to the simple estimate in Eq. (13).

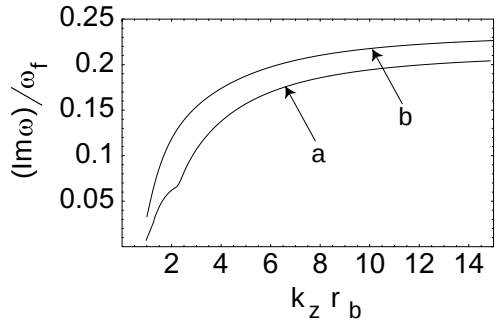

Figure 2: Plots of the normalized growth rate $(Im\omega)/\omega_f$ versus $k_z r_b$ for $\bar{\nu}/\nu_0 = 0.3$, $T_{||b}/T_{\perp b} = 0$ and m=0 (curve a) and m=1 (curve b).

where $n_b^0(r) = \int d^3p f_b^0(r, \mathbf{p})$ is the equilibrium number density of beam particles. We also assume that the beam is located inside a perfectly conducting cylindrical pipe with radius r_w. Furthermore, setting $\phi^0(r = 0) = 0$, the constant $\widehat{n}_b$ occurring in Eq. (14) can be identified with the on-axis density $n_b^0(r = 0)$, and the constants $T_{\perp b}$ and $T_{\|b}$ can be identified with the transverse and longitudinal temperatures (energy units), respectively.

The results obtained with this two codes are in good agreement. We illustrate here some typical results.

Typical numerical results obtained using the bEASt code are presented in Figs. 1 – 3 for the case where $r_w = 3r_b$.

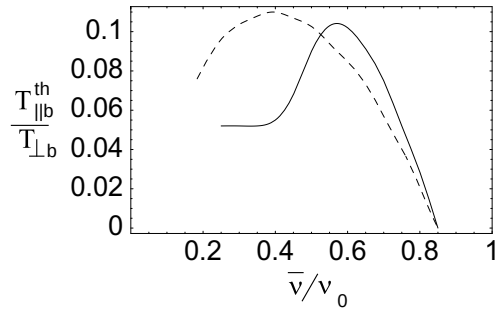

Figure 3: The longitudinal threshold temperature $T_{||b}^{th}$ for the onset of instability normalized to the transverse temperature $T_{\perp b}$ is plotted versus normalized tune depression $\bar{\nu}/\nu_0$ for two values of the azimuthal mode number, $m = 0$ (solid line) and $m = 1$ (dotted line).

Figure 1 shows the normalized growth rate $(Im\omega)_{max}/\omega_f$ and real frequency $(Re\omega)_{max}/\omega_f$ at maximum growth plotted versus the normalized tune depression $\bar{\nu}/\nu_0$ for $T_{||b}/T_{\perp b} = 0$ and azimuthal mode number $m = 0, 1$. For $m = 0$, there are two distinct unstable modes. One is the fastest growing mode for $\bar{\nu}/\nu_0 > 0.55$, and the other is the fastest growing mode for $\bar{\nu}/\nu_0 < 0.55$. The approximate expression [Eq. (13)] for the normalized growth rate $(Im\omega)_{max}/\omega_f$ is also plotted in Fig. 1 a (thick solid curve) for comparison. The $m = 1$ dipole mode has the highest growth rate, $(Im\omega)/\omega_f \simeq 0.34$, for $\bar{\nu}/\nu_0 \simeq 0.62$. The instability is absent for $\bar{\nu}/\nu_0 > 0.82$ for the choice of parameters in Fig. 1. The real frequency $(Re\omega)/\omega_f$ of the unstable mode with azimuthal number $m = 1$ is zero, and is not plotted in Fig. 1. Moreover, the real frequency is plotted only for the most unstable modes in Fig. 1b.

Figure 2 shows the normalized growth rate $(Im\omega)/\omega_f$ plotted versus the normalized wavenumber $k_z r_b$ for normalized tune depression $\bar{\nu}/\nu_0 = 0.3$ and initial temperature ratio $T_{\|b}/T_{\perp b} = 0.0$. The curves (a) and (b) correspond to azimuthal mode numbers $m = 0$ and $m = 1$, respectively. As expected, the instability is present only for short-wavelength perturbations with $k_z^2 r_b^2 > 1$. The effect of finite $T_{\|b}$ (not shown [9, 10, 11, 12]) is to introduce a finite bandwidth in $k_z r_b$ for the instability, since the modes with large values of $k_z r_b$ are stabilized by longitudinal Landau damping in velocity space. Also, the unstable dipole mode with $m = 1$ is purely growing.

An important characteristic of the instability is the longitudinal threshold temperature $T_{||b}^{th}$ for the onset of instability normalized to the transverse temperature $T_{\perp b}$. This quantity is plotted in Fig. 3 versus the normalized tune depression $\bar{\nu}/\nu_0$ for the two values of azimuthal mode number corresponding to $m = 0, 1$. Note from Fig. 3 that the maximum threshold value, $T_{||b}^{th}/T_{\perp b} = 0.11$, is achieved for moderately intense beams with $\bar{\nu}/\nu_0 = 0.4$.

Figures 4-8, obtained using the BEST simulation code, illustrate the nonlinear stage of the instability for a beam with $\bar{\nu}/\nu_0 = 0.6$ and initial temperature ratio $T_{||b}/T_{\perp b} =$

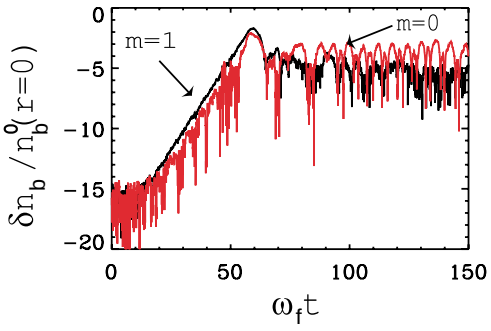

Figure 4: The time history of the two azimuthal components of the density perturbation is shown for m=0 (red), and m=1(black).

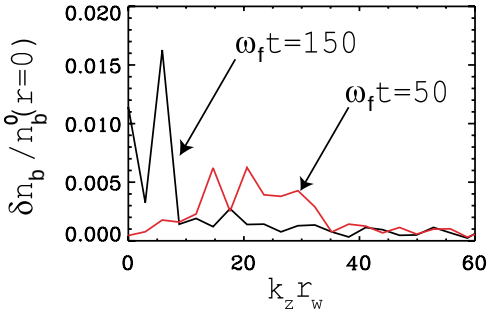

Figure 5: Fourier spectra of the density perturbation δn_b plotted versus $k_z r_w$ at times $\omega_f t = 50$ and $\omega_f t = 150$.

10^{-4}. Figure 4 shows the time history of the two azimuthal components of the density perturbation corresponding to m=0 (red), and m=1(black). As can be seen from Fig. 4, the $m = 1$ mode dominates during the linear stage of the instability, whereas the $m = 0$ mode becomes dominant after the instability has nonlinearly saturated. During the linear stage of the instability, the two modes have frequencies $\omega = 0$ for $m = 1$, and $\omega = 0.55\omega_f$ for $m = 0$. During the nonlinear stage, the frequency of the dominant $m = 0$ mode is almost doubled to $\omega \simeq \omega_f$. Figure 5 shows Fourier spectra of the density perturbation δn_b plotted versus $k_z r_w$ at two different times corresponding to the end of the lin-

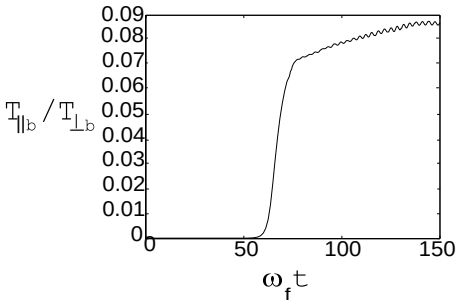

Figure 6: Plot of effective longitudinal temperature $T_{||b} \equiv m_b < v_{||}^2 >$ as a function of time.

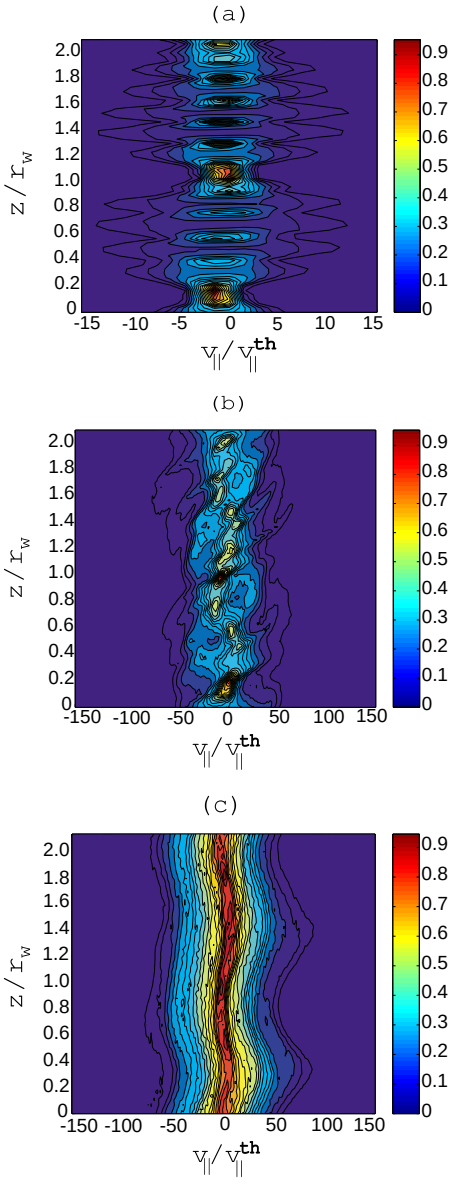

Figure 7: Contour plots in longitudinal phase space of the beam at times (a) $\omega_f t = 65$, (b) $\omega_f t = 75$, and (c) $\omega_f t = 150$.

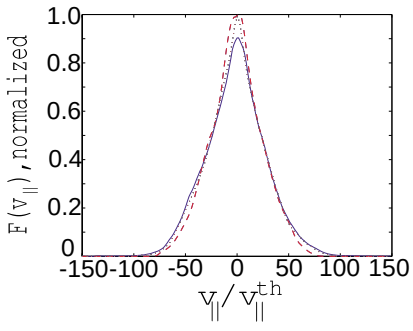

Figure 8: Plots of z-averaged longitudinal velocity distribution at times $\omega_f t = 75$ (red dashed line), $\omega_f t = 100$ (red dotted line) and $\omega_f t = 150$ (solid blue line).

ear stage ($\omega_f t = 50$), and the fully developed nonlinear stage ($\omega_f t = 150$). Initially, the instability is excited over a wide range of longitudinal wavenumbers $k_z r_b > 1$ (see also Fig. 2). During the nonlinear stage, the spectra shifts into the long-wavelength region with $k_z r_b \sim 2$.

Figure 6 shows the behavior of the effective longitudinal temperature $T_{||b} \equiv m_b < v_{||}^2 >$ as a function of time. Comparing with Figure 4, note that the longitudinal temperature stays almost constant during the entire linear stage of the instability, growing super-exponentially during a short time period $50 < \omega_f t < 70$, and then slowly increasing until reaching a constant level $T_{||b}/T_{\perp b} \simeq 0.088$ at time $\omega_f t \sim 150$. The temperature behavior is better illustrated by examining the longitudinal phase space of the beam. Figure 7 shows the contour plots in longitudinal phase space at times (a) $\omega_f t = 65$, (b) $\omega_f t = 75$, and (c) $\omega_f t = 150$. Since the linear stage of instability is dominated by the $m = 1$ mode with zero real frequency, and a wide range of longitudinal wavenumbers, at time $\omega_f t = 65$ the entire distribution is trapped inside the region of velocity space corresponding to $|\delta v| \leq \sqrt{2e_b \delta\phi/m_b} = (\omega_{pb}/k_z)\sqrt{2\delta n_b/n_b^0} \simeq \gamma/k_z^{min}$, where $\gamma \simeq 0.25\omega_f$ is the linear growth rate, and $k_z^{min} r_b \sim 2$ is the smallest wavenumber with appreciable growth rate. During the time interval $50 < \omega_f t < 70$, particles are accelerated longitudinally and fill the trapped region of phase space. During the acceleration phase, the particle velocities are randomly scattered by the many waves excited, which lead to a quasi-linear mixing in phase space [Fig. 7 (b)] by time $\omega_f t = 75$. During remaining time, the nonlinear interactions lead to more mixing and an eventual shift of the oscitation spectra into the $m = 0$ mode and into long-wavelength modes with $k_z r_b \sim 2$ [Fig. 7 (c)]. The final distribution has the clear signature of a nonlinear $m = 0$ mode with almost single-mode excitation at wavelength $\lambda \simeq r_w = 3r_b$ and frequency $\omega \simeq \omega_f$. This wave has a resonant longitudinal velocity $v_w = \omega r_b/(k_z r_b) = v_\perp^{th}(\omega/\omega_f)/(k_z r_b)/(\bar{\nu}/\nu_0) \simeq 0.83 v_\perp^{th} = 83 v_{||0}^{th}$ clearly visible in Fig. 7 (c), with a negligible number of trapped particles.

Figure 8 show the z-averaged longitudinal velocity distribution plotted at times $\omega_f t = 75$ (red dashed line), $\omega_f t = 100$ (red dotted line) and $\omega_f t = 150$ (solid blue line). The velocity distribution becomes almost stationary after time $\omega_f t > 120$, notwithstanding the obvious mode structure that is still clearly evident in the phase-space contour plot. Evidently, the shape of the longitudinal velocity distribution is not Gaussian, but has a triangular shape in Fig. 8.

CONCLUSIONS

To summarize, we have generalized the analysis of the classical Harris instability to the case of a one-component intense charged particle beam with anisotropic temperature. The instability is kinetic in nature and is due to the coupling of the particles' transverse betatron motion with the longitudinal plasma oscillations excited by the perturbation. For a long, coasting beam, the delta-f particle-in-cell code BEST and the eighenmode code bEASt have been used to determine detailed 3D stability properties over a wide range of temperature anisotropy and beam intensity. We have also used the delta-f particle-in-cell code BEST to study the nonlinear evolution and saturation of the instability. The nonlinear saturation is governed by longitudinal particle trapping by a spectrum (not just a single wave) of fast-growing waves with a broad band of longitudinal wavenumbers and zero oscillation frequency. The presence of many waves leads to the nesting and overlapping of particle resonances in longitudinal phase space, and as a consequence, to the fast randomization of the trapped-particle distribution and longitudinal heating. The nonlinear interactions lead to the shift of the waves spectrum into the long-wavelength region ($m = 1 \rightarrow m = 0$ and $k_z r_b \rightarrow 2$). The final longitudinal velocity distribution is not Maxwellian and can be characterized by a remnant temperature anisotropy ($T_{||b}/T_{\perp b} \simeq 0.09$), where $T_{||b} \equiv m_b < v_{||}^2 >$. A very interesting feature of the nonlinear saturation is the formation of a stable, longitudinal, nonlinear BGK-like wave structure with a negligible number of trapped particles.

REFERENCES

[1] E. G. Harris, Phys. Rev. Lett. **2**, 34 (1959).

[2] T. -S. Wang, and L. Smith, Part. Accel. **12**, 247 (1982).

[3] T. -S. Wang, Phys. Rev. ST Accel. Beams **7**, 024201 (2004).

[4] A. Friedman, D. A. Callahan, D. P. Grote, A. B. Langdon, and I. Haber, Bull. Am. Phys. Soc. **35**, 2121 (1990).

[5] A. Friedman, R. O. Bangerter, D. A. Callahan, D. P. Grote, A. B. Langdon, and I. Haber, Proceedings of the 2nd European Particle Accelerator Conference, 1699 (1990), edited by P. A. Martin, Vol 2.

[6] S. M. Lund, D. A. Callahan, A. Friedman, D. P. Grote, I. Haber, and T. F. Wang, *Proceedings of XIX International Linear Accelerator Conference* Chicago, 1998, edited by C. E. Eyberger, R. C. Pardo and M. M. White (Argone National Laboratory, Argone, Illinois, 1998). p.372.

[7] S. M. Lund, J. J. Barnard, G. D. Craig, A. Friedman, D. P. Grote, T. S. Sangster, W. M. Sharp, S. Eylon, T. T. Fessenden, E. Henestroza, S. Yu, and I. Haber, Nuclear Instruments and Methods in Physics Research A **415**, 345 (1998).

[8] I. Haber, A. Friedman, D. P. Grote, S. M. Lund, and R. A. Kishek, Phys. Plasmas **6**, 2254 (1999).

[9] E. A. Startsev, R. C. Davidson and H. Qin, Phys. Plasmas **9**, 3138 (2002).

[10] E. A. Startsev, R. C. Davidson and H. Qin, Laser and Particle Beams **20**, 585 (2002).

[11] E. A. Startsev, R. C. Davidson and H. Qin, Phys. Rev. ST Accel. Beams **6**, 084401 (2003).

[12] E. A. Startsev, R. C. Davidson and H. Qin, Nucl. Inst. Meth. in Phys. Res. A, in press (2005).

[13] H. Qin, R. C. Davidson and W. W. Lee, Phys. Rev. ST Accel. Beams **3**, 084401 (2000); **3**, 109901 (2000).